Understanding localized surface plasmon resonance with propagative surface plasmon polaritons in optical nanogap antennas

Hongwei Jia,[1,2] Fan Yang,[3] Ying Zhong,[4] and Haitao Liu[1,*]

[1]*Key Laboratory of Optical Information Science and Technology, Ministry of Education, Institute of Modern Optics, Nankai University, Tianjin 300071, China*
[2]*SZU-NUS Collaborative Innovation Center for Optoelectronic Science & Technology, Key Laboratory of Optoelectronic Devices and Systems of Ministry of Education and Guangdong Province, College of Optoelectronic Engineering, Shenzhen University, Shenzhen 518060, China*
[3]*State Key Laboratory of Low Dimensional Quantum Physics, Department of Physics, Tsinghua University, Beijing 100084, China*
[4]*State Key Laboratory of Precision Measuring Technology and Instruments, Tianjin University, Tianjin 300072, China*
**Corresponding author: liuht@nankai.edu.cn*

Received August 17, 2016; revised October 7, 2016; accepted October 9, 2016;
posted October 13, 2016 (Doc. ID 273965); published November 9, 2016

The plasmonic nanogap antenna is an efficient radiating or receiving optical device. The resonance behavior of optical antennas is commonly attributed to the excitation of a localized surface plasmon resonance (LSPR), which can be theoretically defined as the quasi-normal mode (QNM). To clarify the physical origin of the LSPR, we build up an analytical model of the LSPR by considering a multiple scattering process of propagative surface plasmon polaritons (SPPs) on the antenna arms. The model can comprehensively reproduce the complex eigenfrequency and the field distribution of QNMs of the antenna, unveiling that the LSPR arises from a Fabry–Perot resonance of SPPs. By further applying the complex pole expansion theorem of meromorphic functions, the field of the antenna under illumination by a nearby dipole emitter can be analytically expanded with QNMs, which well predicts the frequency response of the enhancement factor of radiation. The present model establishes explicit relations between the concepts of the LSPR and the propagative SPP and integrates the advantages of the Fabry–Perot and QNM formalisms of nanogap antennas.

OCIS codes: (240.6680) Surface plasmons; (260.5740) Resonance; (050.6624) Subwavelength structures.
http://dx.doi.org/10.1364/PRJ.4.000293

1. INTRODUCTION

Resonant optical antennas are important devices that can efficiently accelerate the radiation of emitters such as molecules or quantum dots placed nearby [1–6] or, reciprocally, allow giant enhancement of the near field under far-field illumination [7–12]. By controlling the geometrical parameters to fulfill resonance conditions, optical antennas can be widely used in nonlinear optics [13,14], white light supercontinuum generation [7], single-emitter fluorescence enhancement [1,3], and surface enhanced Raman scattering [15–17]. The enhancement of field or emission is especially stringent in nanogaps formed at the mouth of metal nanoparticles that are nearly in contact, so that nanogap antennas have many established applications ranging from electron tunneling microscopy, nanocatalysis, and Raman spectroscopy to disruptive electronics and light emission [10]. The resonance enhancement is commonly attributed to an excitation of localized surface plasmon resonance (LSPR) as the illumination frequency matches the eigenfrequency of the LSPR [12,18–21].

For the nanogap antenna composed of two strongly coupled individual nanowires, the LSPR is classified into bonding and antibonding modes with opposite field symmetries [18,19]. Theoretically, the LSPR can be defined as the quasi-normal mode (QNM) by treating the metallic nanoantenna as an open cavity [21]. The QNM is a solution of source-free Maxwell's equations with an eigenfrequency of complex value due to the cavity loss [22]. The formalism of QNMs is a powerful tool able to provide an analytical description of the frequency response of open or lossy resonators [18–23] and shows great advantages over standard full-wave solvers that repeat the entire calculation for different frequencies [12]. However, presently the QNMs of antennas are commonly obtained via full-wave numerical calculations [20,21,24–29]. Too few reports provide a comprehensive analytical description of QNMs (for instance, for some special cavities such as one-dimensional cavities and microspheres [30,31], the eigenfrequency and field of the QNM are analytical), which blocks a further understanding of the physical origin of QNMs and thus an efficient design of antenna devices.

To achieve a physical understanding of the resonance behaviors of nanoantennas, different theoretical approaches have been reported. In the lumped-elements circuit model, the antenna is treated as a circuit composed of resistors, inductors, and capacitors, so that the resonance is intuitively understood as the resonance of the AC current in the circuit [32,33]. The temporal coupled-mode theory is established by considering the coupling between the eigenmodes and the input and output ports of the resonator, and it can be readily used for analyzing the Fano or Lorentzian line shape of the frequency response of antenna arrays [34,35]. However, in

these theories, surface plasmon polaritons (SPPs) do not appear in an explicit form. The SPP can be defined as a waveguide mode that propagates along a metal–dielectric interface [36–39] and is conceptually different from the LSPR. A counterexample can be found for the analysis of metallic-sphere dimmers by showing how SPPs propagate at the metal surface and are slowed down at the dimmer mouth to build a hot spot [40]. SPP Fabry–Perot models have been developed for antennas composed of a single wire, in which SPPs are bouncing back and forth between the arm facets that act as mirrors [41–44]. Recently, the Fabry–Perot model has been extended to nanogap antennas with two arms by including the SPP hopping from one arm to the other and the SPP reflection at the gap [5,11]. The extended model, which relies on the *ab initio* calculation of a few elementary SPP scattering coefficients, has been shown to comprehensively and accurately reproduce many antenna characteristics, for example, scattering cross section, near-field enhancement factor, Purcell factor, and far-field radiation pattern. However, since the excitation and scattering processes of SPPs depend on the illumination frequency in an implicit way, the Fabry–Perot model cannot provide an analytical description of the frequency response of the antenna.

In this paper, we combine the Fabry–Perot and QNM formalisms, capitalizing on the intuitive force of the former and the frequency-analyticity of the latter, to propose an insightful and effective theoretical treatment of nanogap antennas. For that purpose, we build up an SPP Fabry–Perot model for the QNM of nanogap antennas by considering a multiple scattering process of SPPs on the antenna arms. The existence of slightly damped QNMs that cause the resonance nature of nanogap antennas is demonstrated with the model by seeking the solutions of two transcendental equations. The model sets a solid electromagnetic foundation for the intuitive picture that the LSPR (i.e., QNM) of the antenna actually arises from the Fabry–Perot resonance of SPPs at the complex eigenfrequency. With a few assumptions on the frequency dependence of the field and with the use of complex pole expansion of meromorphic functions (Mittag–Leffler theorem), the field of the nanogap antenna excited by a nearby point emitter can be expanded upon the basis of QNMs, thus providing an analytical description of the frequency response of the field. For calculating the Purcell factor, the model provides a new analytical expression of the mode volume of QNM in terms of the SPP scattering coefficients, which avoids the difficulty in calculating the mode volume caused by the divergence of the QNM field at infinity that was overcome recently [20]. The present model establishes explicit relations between the concepts of the LSPR and the propagative SPP, and it integrates the advantages of the Fabry–Perot and QNM formalisms in understanding the resonance of nanogap antennas, which may inspire new design strategies of antenna devices with different geometries [1,45–50].

2. SPP MODEL OF LSPR FOR NANOGAP ANTENNAS

As shown in Fig. 1(a), the considered nanogap antenna is formed by two arms of gold nanowires (with length L) separated by a nanogap (with width $w = 0.03$ μm). The nanowires have a square cross section with a side length $D = 0.04$ μm. The antenna is surrounded by air (refractive index $n_a = 1$) without a substrate for simplicity. For solving QNMs at complex frequencies, the gold permittivity at complex frequencies is obtained through an analytical continuation by using an analytical expression obtained with a polynomial fitting of the experimental data of the gold permittivity at real frequencies [51]. Next we will try to derive analytical expressions for the field and the eigenfrequency of the QNMs based on a multiple scattering formalism of SPPs [5]. Since the transversal size of the antenna arms is much smaller than the wavelength, only one fundamental SPP mode is propagative and bounded on the antenna arms that are treated as x-invariant waveguides [36,37]. All other waveguide modes on antenna arms are either evanescent or unbounded and thus are neglected in the model. In view of the multiple scattering processes of SPPs as sketched in Fig. 1(a), the field of QNM of the antenna can be expressed as

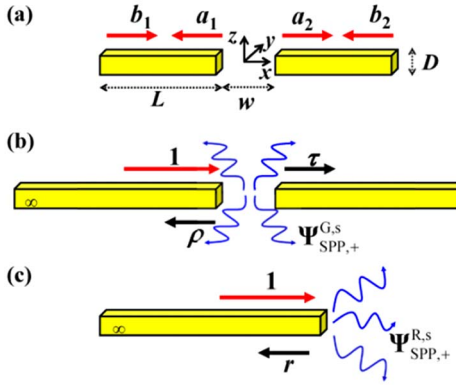

Fig. 1. (a) Sketch of the nanogap antenna. The antenna is composed of two gold nanowire arms of length L (with a square cross section of side length $D = 40$ nm) separated by a nanogap (gap width $w = 30$ nm). a_1, a_2, b_1, and b_2 are the complex amplitude coefficients of SPPs at the complex eigenfrequency of QNMs. (b) and (c) definitions of SPP scattering coefficients ρ, τ, and r and scattered fields $\mathbf{\Psi}^{G,s}_{SPP,+}$ and $\mathbf{\Psi}^{R,s}_{SPP,+}$ used in the model.

$$\mathbf{\Psi}_{QNM} = a_1 u \mathbf{\Psi}^{L,s}_{SPP,-} + a_2 u \mathbf{\Psi}^{R,s}_{SPP,+} + b_1 u \mathbf{\Psi}^{G,s}_{SPP,+} + b_2 u \mathbf{\Psi}^{G,s}_{SPP,-}, \tag{1}$$

where $\mathbf{\Psi} = [\mathbf{E}, \mathbf{H}]$ denotes both the electric- and the magnetic-field vectors. $\mathbf{\Psi}^{G,s}_{SPP,+}$ [Fig. 1(b)] and $\mathbf{\Psi}^{R,s}_{SPP,+}$ [Fig. 1(c)] denote the fields scattered at the nanogap and at the right termination of the antenna for an incident right-going SPP, respectively. $\mathbf{\Psi}^{G,s}_{SPP,-}$ and $\mathbf{\Psi}^{L,s}_{SPP,-}$ are defined similarly for an incident left-going SPP. $u = \exp(ik_{0,c} n_{eff} L)$ is the phase shift of the SPP accumulated over one antenna arm ($k_{0,c} = \omega_c/c$, ω_c being the complex angular frequency of the QNM, c being the light speed in vacuum, and n_{eff} being the complex effective index of the SPP). Equation (1) is written with the view that the field of the QNM contains four parts: the two fields scattered at the two terminations for incident SPPs propagating away from the gap (with coefficients a_1 and a_2 and a damping u) and the two fields scattered at the nanogap for incident SPPs propagating toward the gap (with coefficients b_1 and b_2 and a damping u). The scattered fields ($\mathbf{\Psi}^{G,s}_{SPP,+}$, $\mathbf{\Psi}^{R,s}_{SPP,+}$, $\mathbf{\Psi}^{G,s}_{SPP,-}$, and $\mathbf{\Psi}^{L,s}_{SPP,-}$) and n_{eff} can be calculated independently with the full-wave aperiodic Fourier modal method (a-FMM) [5,52,53]. The efficiency and accuracy of the a-FMM compared with other full-wave

solvers of Maxwell's equations such as the finite element method or finite difference time domain method has been confirmed [54]. In Eq. (1), the unknown amplitude coefficients a_1, a_2, b_1, and b_2 of SPPs [Fig. 1(a)] can be determined by solving a set of coupled SPP equations:

$$a_1 = b_1 u\rho + b_2 u\tau, \tag{2a}$$

$$a_2 = b_1 u\tau + b_2 u\rho, \tag{2b}$$

$$b_1 = a_1 ur, \tag{2c}$$

$$b_2 = a_2 ur, \tag{2d}$$

where ρ and τ denote the SPP reflection and transmission coefficients at the nanogap [38] [Fig. 1(b)], and r is the SPP reflection coefficient at the antenna termination [39] [Fig. 1(c)]. Here ρ, τ, and r are calculated in a rigorous manner as the scattering matrix elements [5,55] with the full-wave a-FMM [52,53] without relying on any assumption or any fitting of rigorous data, which ensures a solid electromagnetic foundation of the present model. Equations (2) can be understood intuitively. For the first equation, for instance, the coefficient a_1 results from two contributions: the first contribution from the reflection (ρ) of an incident right-going SPP (with coefficient b_1 and damping u) on the left arm, and the second contribution from the transmission (τ) of an incident left-going SPP on the right arm (with coefficient b_2 and damping u). Note that no excitation terms appear in Eqs. (2), since the QNM is the eigensolution of Maxwell's equations without source. Equations (2) form a set of homogeneous linear equations of a_1, a_2, b_1, and b_2. To ensure the existence of nontrivial solutions of Eqs. (2), the determinant of the coefficient matrix should be zero, which yields

$$u^2 r(\rho + \tau) = 1, \tag{3a}$$

$$u^2 r(\rho - \tau) = 1. \tag{3b}$$

Equations (3) form two transcendental equations for determining the complex eigenfrequencies of QNMs. Since ρ, τ, and r are independent of the antenna arm length L and $u = \exp(ik_{0,c}n_{\text{eff}}L)$ depends on L analytically, Eqs. (3) could be more computationally efficient in solving the QNM eigenfrequencies than full-wave calculations, especially for large values of L. With Eqs. (3a) or (3b) inserted into Eqs. (2), we can obtain the SPP coefficients $a_1 = a_2$, $b_1 = b_2$, or $a_1 = -a_2$, $b_1 = -b_2$, respectively. The two solutions correspond to QNMs with different symmetries of field, termed as the bonding mode and antibonding mode, respectively [18,19]. With the two solutions inserted into Eq. (1), we finally obtain the analytical expressions for the field distribution of the bonding and antibonding QNMs (with normalization $a_1 = u^{-1}$):

$$\boldsymbol{\Psi}^{\text{b}}_{\text{QNM}} = \boldsymbol{\Psi}^{\text{L,s}}_{\text{SPP},-} + \boldsymbol{\Psi}^{\text{R,s}}_{\text{SPP},+} + ur\boldsymbol{\Psi}^{\text{G,s}}_{\text{SPP},+} + ur\boldsymbol{\Psi}^{\text{G,s}}_{\text{SPP},-}, \tag{4a}$$

$$\boldsymbol{\Psi}^{\text{a}}_{\text{QNM}} = \boldsymbol{\Psi}^{\text{L,s}}_{\text{SPP},-} - \boldsymbol{\Psi}^{\text{R,s}}_{\text{SPP},+} + ur\boldsymbol{\Psi}^{\text{G,s}}_{\text{SPP},+} - ur\boldsymbol{\Psi}^{\text{G,s}}_{\text{SPP},-}. \tag{4b}$$

Equations (4) can be further simplified at some specific positions such as in the nanogap or near the antenna terminations, and details can be found in Appendix D. To seek the solution, Eqs. (2) can be rewritten as

$$k_{0,c} = -\frac{\ln(|r||\rho + \tau|) + i[\arg(r) + \arg(\rho + \tau) - 2M\pi]}{i2n_{\text{eff}}L}, \tag{5a}$$

$$k_{0,c} = -\frac{\ln(|r||\rho - \tau|) + i[\arg(r) + \arg(\rho - \tau) - 2N\pi]}{i2n_{\text{eff}}L}, \tag{5b}$$

where M and N are integers that correspond to different orders of QNMs, and arg() denotes the argument. In view of the propagative nature of the SPP mode, n_{eff} is approximately a real number, so that $\text{Im}(k_{0,c}) \approx \ln(|r||\rho \pm \tau|)/(2n_{\text{eff}}L)$. It has been shown that $|r| \approx 1$ for the SPP reflection at the antenna termination [39], and $|\rho \pm \tau| \approx 1$ for the SPP transmission and reflection at the nanogap due to energy conservation [38]. Thus we have $\text{Im}(k_{0,c}) \approx 0$, implying the existence of slightly damped QNMs that cause the resonance nature of the nanogap antenna. In fact, a crude evaluation of $k_{0,c}$ can be obtained by calculating the right side of Eqs. (5) [denoted by $g(k_{0,c})$] at a certain frequency, in view that ρ, τ, r, n_{eff}, and thus $g(k_{0,c})$ are slowly varying functions of $k_{0,c}$. The accuracy of this evaluation can be further improved with the iteration formula $k^m_{0,c} = g(k^{m-1}_{0,c})$ [11]. To seek the solution of Eqs. (5) in a rigorous manner, we can solve the nonlinear equation $f(k_{0,c}) = k_{0,c} - g(k_{0,c}) = 0$ with classical numerical techniques such as the linear interpolation method [56]. By setting two initial values $k^0_{0,c}$ and $k^1_{0,c}$ and approximating $f(k_{0,c})$ as a linear form $f(k_{0,c}) = p + qk_{0,c}$, a sequence of $k^m_{0,c}$ can be obtained by solving $p + qk^m_{0,c} = 0$, which approaches the exact solution rapidly as m increases. Equations (5) are superior to Eqs. (3) for seeking solutions since for designated integers M or N, the solution of Eqs. (5) is commonly unique and thus not sensitive to the initial values $k^0_{0,c}$ and $k^1_{0,c}$. While Eqs. (3) have an infinite number of solutions, so that the solved eigenfrequency is the one closest to the initial values. Taking the real part of both sides of Eqs. (5) after multiplying by $2n_{\text{eff}}L$, we obtain

$$2\,\text{Re}(k_{0,c}n_{\text{eff}})L + \arg(r) + \arg(\rho + \tau) = 2M\pi, \tag{6a}$$

$$2\,\text{Re}(k_{0,c}n_{\text{eff}})L + \arg(r) + \arg(\rho - \tau) = 2N\pi. \tag{6b}$$

Equations (6) show that at the complex eigenfrequency ω_c of QNMs, the phase shift of SPPs that propagate back and forth over one round on the antenna is multiples of 2π, indicating that the QNM (i.e., LSPR) originates from a Fabry–Perot resonance of SPPs at the eigenfrequency.

Now we check the validity of the model through a comparison to the full-wave numerical data. We first reproduce the eigenfrequency ω_c of the QNM of the antenna by solving Eqs. (5), as shown in Table 1 for antenna lengths $L = 0.2$ and 0.6 μm. For solving the QNM with the full-wave a-FMM, a point emitter with complex frequency is placed in the vicinity of the antenna. In view of the divergence of the excited field $F(\omega)$ as the emitter frequency ω approaches the eigenfrequency of QNMs, the QNMs can be obtained by solving a nonlinear equation $1/F(\omega) = 0$ (with the linear interpolation method) [11,56]. The solution of $1/F(\omega) = 0$ is commonly not unique and depends sensitively on the initial value,

Table 1. Complex Eigenfrequencies ω_c ($\lambda_c = 2\pi c/\omega_c$) of QNMs

L (μm)	M or N	λ_c (SPP model)	λ_c (a–FMM)
0.2	$M=1$	$0.9776+0.0574i$	$0.9635+0.0925i$
	$N=1$	$0.8068+0.0226i$	$0.8089+0.0233i$
0.6	$M=1$	$2.4262+0.1789i$	$2.3928+0.2823i$
	$N=1$	$1.9468+0.0921i$	$1.9525+0.0976i$
	$M=2$	$1.0830+0.0427i$	$1.0920+0.0455i$
	$N=2$	$0.9782+0.0260i$	$0.9783+0.0251i$
	$M=3$	$0.7707+0.0166i$	$0.7716+0.0159i$
	$N=3$	$0.7410+0.0141i$	$0.7410+0.0141i$
	$M=4$	$0.6638+0.0115i$	$0.6636+0.0117i$
	$N=4$	$0.6522+0.0103i$	$0.6522+0.0103i$

which causes difficulty in finding all QNMs within the wavelength range of interest. However, as mentioned earlier, this difficulty can be largely overcome by solving Eqs. (5) of the model due to their uniqueness of solution. It is seen that the eigenfrequencies obtained with the model agree well with the full-wave a-FMM results. Only for the $M=1$ order QNM does the predicted eigenfrequency slightly deviate from the a-FMM result (especially the imaginary part), which is due to the impact of surface waves other than SPPs that are neglected in the model (see Appendix A for details).

Then we will reproduce the field of QNMs with Eqs. (4) of the model. The results for QNMs of different orders with antenna length $L=0.6$ μm are shown in Fig. 2 (obtained in plane $y=0$). Note that the fields of QNMs calculated with the a-FMM are normalized by setting the left-going SPP coefficient on the left arm to be u^{-1}, which is consistent with the QNM normalization in Eqs. (4) of the model. The QNM field distributions predicted by the model (right column) agree well with the full-wave results (left column). This is true even for the $M=1$ order QNM, for which the model cannot predict the eigenfrequency as accurate (Table 1), and the reason lies in the consistent normalization of the QNM field for the model and for the a-FMM. In Figs. 2(a)–2(f), the first two parts show the distributions of $\mathrm{Re}(E_x)$ for $M=1, 2, 3$ and $N=1, 2, 3$ orders of QNMs, exhibiting different field symmetries of the bonding and antibonding modes as indicated earlier with Eqs. (4). Other parts of Fig. 2 show the distributions of the electric field amplitude ($|\mathbf{E}|=\sqrt{|E_x|^2+|E_y|^2+|E_z|^2}$). It is seen that for the bonding modes ($M=1, 2, \ldots$), the field in the nanogap is very strong, but the field in the gap is nearly zero for the antibonding modes ($N=1, 2, \ldots$). The number of field nodes on the antenna arms increases with the increase of the resonance order M or N, which is due to an interference of the two counterpropagating SPPs on each arm of the antenna. The field of QNMs for antenna length $L=0.2$ μm is provided in Appendix B.

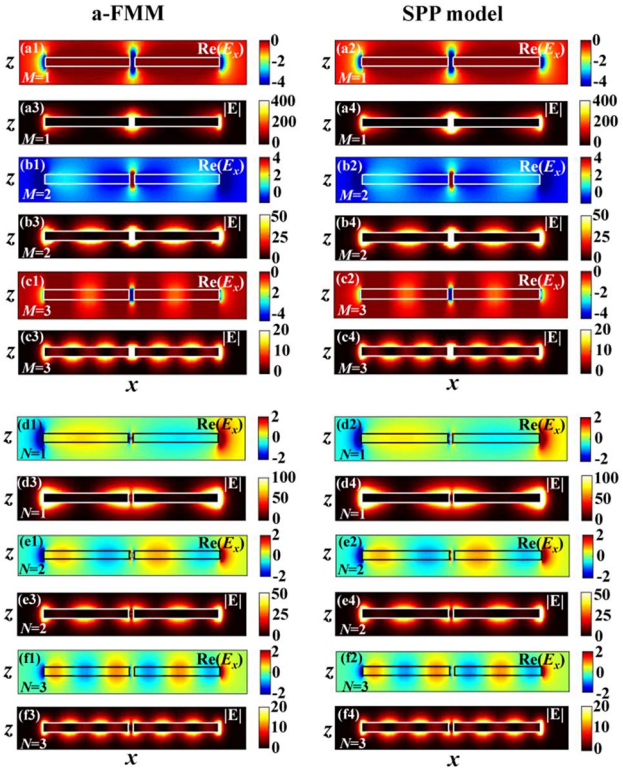

Fig. 2. Field distributions of QNMs for antenna arm length $L=0.6$ μm. The left and right columns show the results obtained with the full-wave a-FMM and with the SPP model, respectively. (a)–(c) show the bonding QNMs for $M=1, 2, 3$, respectively, where the electric-field amplitude is defined as $|\mathbf{E}|=\sqrt{|E_x|^2+|E_y|^2+|E_z|^2}$. (d)–(f) show the antibonding QNMs for $N=1, 2, 3$, respectively.

3. REPRODUCING ENHANCEMENT FACTOR OF RADIATION WITH THE MODEL

In previous theories that treat the antenna arms as microcavities of SPPs [5,41,43], the enhancement of the radiation from a dipole emitter in the vicinity of the antenna is attributed to a Fabry–Perot resonance of SPPs. Another interpretation of the radiation enhancement is based on a resonant excitation of the LSPR (i.e., QNM) [18–21]. In this section, we will apply the SPP model of the LSPR established in Section 2 to reproduce the enhancement factor of the radiation of the nanogap antenna, thus establishing explicit relations between the two interpretations.

A. Radiation Enhancement for an Emitter Located in the Nanogap

We first consider the case that an x-polarized electric dipole source (with a current density expressed with Dirac function $\mathbf{J}=\delta(x,y,z)\mathbf{x}$, $\mathbf{x}$ being a unit vector along the x direction) is located at the center of the gap of the antenna, as sketched in Fig. 3(a). The dipole source is used to represent a molecule [1–3] or a quantum dot [4,6] in practical situations. The enhancement factor $F=\Gamma_{\mathrm{tot}}/\Gamma_{\mathrm{air}}$ is used to characterize the acceleration of the spontaneous emission/decay rate of a dipole emitter in the vicinity of nanostructures [57], where Γ_{tot} and Γ_{air} represent the spontaneous emission rates with and without the presence of nanostructures, respectively. For the present case, Γ_{tot} can be calculated with the field at the source position, $\Gamma_{\mathrm{tot}}=-\mathrm{Re}[E_x(\mathbf{r}_0)]/2$ ($\mathbf{r}_0$ being the coordinate of the source), and $\Gamma_{\mathrm{air}}=\eta_{\mathrm{vac}}k_0^2 n_a/(12\pi)$ ($k_0=\omega/c$, $n_a=1$ being the refractive index of air, and η_{vac} being the wave impedance in vacuum). The Purcell factor, which denotes the highest acceleration of the spontaneous emission/decay rate when changing the frequency, the position, and the polarization of the emitter, is required to achieve high values for applications such as high-speed quantum information processing [58] and fluorescence sensing of molecules [59].

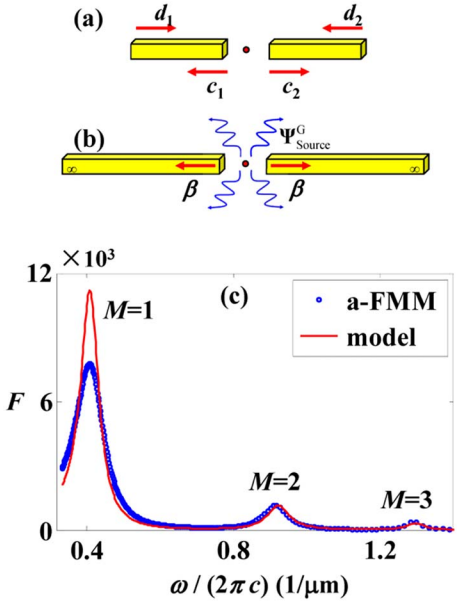

Fig. 3. (a) Definitions of the amplitude coefficients (c_1, c_2, d_1, and d_2) of SPPs excited by an x-polarized electric point source located at the center of the nanogap. (b) Definitions of the SPP excitation coefficient β and scattered field used in the model. (c) Enhancement factor F of radiation plotted as a function of illumination frequency $\omega/(2\pi c)$. Results are obtained with the full-wave a-FMM (blue circles) and the SPP model (red solid curve) for antenna length $L = 0.6$ μm.

To obtain the field under the excitation of the dipole emitter, we use c_1, c_2, d_1, and d_2 to denote the amplitude coefficients of SPPs that propagate back and forth on the antenna arms, as sketched in Fig. 3(a). To solve the unknown SPP coefficients, a set of coupled-mode equations can be written [5]:

$$c_1 = \beta + d_1 u\rho + d_2 u\tau, \tag{7a}$$

$$c_2 = \beta + d_2 u\rho + d_1 u\tau, \tag{7b}$$

$$d_1 = c_1 ur, \tag{7c}$$

$$d_2 = c_2 ur, \tag{7d}$$

where β denotes the excitation coefficient of SPPs by the dipole source [Fig. 3(b)], which can be calculated as the scattering-matrix element [5,53,55] or with the Lorentzian reciprocity relation by sending an incident SPP [see Eq. (C5) in Appendix C]. Other scattering coefficients (ρ, τ, and r) have been defined earlier in Fig. 1. Equations (7) can be understood in a way similar to Eqs. (2). They can be analytically solved as

$$c_1 = c_2 = \frac{\beta}{1 - u^2 r(\rho + \tau)}, \tag{8a}$$

$$d_1 = d_2 = \frac{\beta ur}{1 - u^2 r(\rho + \tau)}. \tag{8b}$$

Then the field excited by the emitter can be expressed as [5]

$$\Psi = \Psi^{G}_{Source} + c_1 u\Psi^{L,s}_{SPP,-} + c_2 u\Psi^{R,s}_{SPP,+} + d_1 u\Psi^{G,s}_{SPP,+} + d_2 u\Psi^{G,s}_{SPP,-}, \tag{9}$$

where Ψ^{G}_{Source} denotes the field excited by the point source for an infinitely long nanowire with a nanogap [see Fig. 3(b)], and other terms ($\Psi^{G,s}_{SPP+}$, $\Psi^{G,s}_{SPP-}$, $\Psi^{R,s}_{SPP+}$ and $\Psi^{L,s}_{SPP-}$) are defined earlier in Fig. 1. Equation (9) is written similar to Eq. (1), except for the first term representing the source excitation. Note that all the quantities on the right side of Eq. (9) depend on the illumination frequency (taking real values) in an implicit form. To seek the frequency response in an analytical form, next we consider to expand the excited field expressed with Eq. (9) upon the basis of QNMs [20,60,61]. Equations (3) and (8) show that as the illumination frequency ω approaches the complex eigenfrequency ω_c of QNMs, the SPP coefficients c_1, c_2, d_1, and d_2 approach infinity, and resultantly, the excited field Ψ in Eq. (9) diverges to infinity. Then we assume that Ψ is a meromorphic function of ω, with the ω_c being the first-order pole of Ψ, and that Ψ is bounded as $|\omega| \to \infty$ in the complex plane. This assumption has been shown to be valid for the field inside or near nanogrooves [62] and will be shown to be valid for the present case of nanogap antennas. According to the complex pole expansion of meromorphic functions (Mittag–Leffler theorem) [62–64], the field Ψ can be expressed analytically with respect to ω:

$$\Psi(\omega) = \Psi(0) + \sum_n \frac{\omega/\omega_{c,n}}{\omega - \omega_{c,n}} \mathbf{p}_n, \tag{10}$$

where $\omega_{c,n}$ denotes the eigenfrequency of the nth order QNM [n can be M or N in Eqs. (5)]. The term $\Psi(0) \approx 0$ in view that at $\omega = 0$ the scattering effect of the finite-size antenna vanishes for an infinitely-large wavelength. $\mathbf{p}_n = \lim_{\omega\to\omega_{c,n}}(\omega - \omega_{c,n})\Psi(\omega)$ is the residue of Ψ at the pole $\omega_{c,n}$. Note that the way of deriving the expansion of Eq. (10) is essentially different from previous methods (such as the Lorentzian reciprocity theorem [20] and the two component expansion method [60,61]) that depend on the assumption of the completeness of QNMs. With Eqs. (8) and (9), we obtain

$$\mathbf{p}_n = \lim_{\omega\to\omega_{c,n}} \frac{\beta u(\omega - \omega_{c,n})}{1 - u^2 r(\rho + \tau)} \times (\Psi^{L,s}_{SPP,-} + \Psi^{R,s}_{SPP,+} + ur\Psi^{G,s}_{SPP,+} + ur\Psi^{G,s}_{SPP,-}), \tag{11}$$

where $\lim_{\omega\to\omega_{c,n}}(\omega - \omega_{c,n})\Psi^{G}_{Source}(\omega)$ is zero since $\Psi^{G}_{Source}(\omega)$ is a nonresonant term. The summation in the last bracket in Eq. (11) is nothing else than the field of the bonding QNM expressed with Eq. (4a), showing that for the emitter at the center of the nanogap, only the bonding QNMs are excited (i.e., $n = M$). The limit in Eq. (11) (with $n = M$) is the type of 0/0 and can be calculated with L'Hospital's rule,

$$\lim_{\omega\to\omega_{c,M}} \frac{\beta u(\omega - \omega_{c,M})}{1 - u^2 r(\rho + \tau)} = \frac{(\beta u)_{\omega=\omega_{c,M}}}{\left[-\frac{4\pi i\omega n_{eff} L}{c}\left(\frac{1}{\omega} + \frac{1}{n_{eff}}\frac{\partial n_{eff}}{\partial\omega}\right) - \frac{1}{r}\frac{\partial r}{\partial\omega} - \frac{1}{\rho+\tau}\frac{\partial(\rho+\tau)}{\partial\omega}\right]_{\omega=\omega_{c,M}}}. \tag{12}$$

With Eqs. (10)–(12), we finally obtain

$$\Psi(\omega) = \sum_M \eta_M(\omega)\Psi^{b}_{QNM,M}, \tag{13}$$

where $\Psi^{b}_{QNM,M}$ is the field of the Mth-order bonding QNM at eigenfrequency $\omega_{c,M}$ [expressed with Eq. (4a)], and η_M is a complex expansion coefficient expressed as

$$\eta_M(\omega)=\frac{\omega/\omega_{c,M}}{\omega-\omega_{c,M}}\times\frac{(\beta u)_{\omega=\omega_{c,M}}}{\left[-\frac{4\pi i\omega n_{\text{eff}}L}{c}\left(\frac{1}{\omega}+\frac{1}{n_{\text{eff}}}\frac{\partial n_{\text{eff}}}{\partial\omega}\right)-\frac{1}{r}\frac{\partial r}{\partial\omega}-\frac{1}{\rho+\tau}\frac{\partial(\rho+\tau)}{\partial\omega}\right]_{\omega=\omega_{c,M}}}. \quad (14)$$

Equation (14) shows that the expansion coefficients of QNMs can be analytically expressed with the SPP scattering coefficients at the eigenfrequency $\omega_{c,M}$. Note that the scattering coefficients (β, r, ρ, τ) and the complex effective index (n_{eff}) of the SPP are calculated at the eigenfrequency (with the full-wave a-FMM), so that they are independent of the illumination frequency ω. Also note that when changing the position and polarization of the point emitter, in Eqs. (13) and (14) only the SPP excitation coefficient β changes and all other parameters do not change. And with the use of reciprocity theorem, β for different emitter positions and polarizations can be obtained with only one full-wave calculation [see Eq. (C5) in Appendix C]. This virtue with the use of reciprocity is analogous to that with the use of reciprocity between a point emitter and QNMs [20]. Equations (13) and (14) provide an analytical description of the frequency response of nanogap antennas along with an intuitive multiple scattering picture of SPPs. The selection of the QNMs in the expansion of Eq. (13) is determined by the frequency range of interests.

For the case that the antenna resonance is dominated by a single QNM, the Purcell factor can be expressed as [20] $F_P=3(4\pi^2)^{-1}(\lambda_0/n_a)^3\,\text{Re}(Q/V)$, where λ_0 is the vacuum wavelength at resonance, n_a is the refractive index of environment ($n_a=1$ in air), and $Q=-\text{Re}(\omega_c)/[2\text{Im}(\omega_c)]$ and V are the quality factor and the complex-valued mode volume of the dominant QNM, respectively. With Eq. (14), the mode volume V can be expressed analytically with the SPP scattering coefficients (a detailed derivation can be found in Appendix C). This avoids the difficulty caused by the divergence of the QNM field at infinity when calculating the mode volume as an integral of the QNM field over the whole space. This difficulty has been recently overcome by introducing perfectly matched layers to treat the divergence of the QNM field at infinity [20].

Now we check the validity of the model in predicting the enhancement factor F of radiation. The results obtained with the full-wave a-FMM and with the model [Eqs. (13) and (14)] are shown in Fig. 3(c) with blue circles and red solid curves, respectively, with antenna length $L=0.6$ μm. It is seen that the model predictions agree well with the a-FMM data except for an observable deviation at the resonance corresponding to the $M=1$ order QNM, which is due to the impact of surface waves other than SPPs (see Appendix A for details). As shown explicitly by Eqs. (13) and (14), the enhancement factor F of emission peaks at $\omega=\text{Re}(\omega_{c,M})$, which is confirmed by the results in Fig. 3(c). In view of $\omega_{c,M}\approx\text{Re}(\omega_{c,M})$, since $\text{Im}(\omega_{c,M})$ is a small number (as shown in Table 1), Eq. (6a) at $\omega=\omega_{c,M}$ then approximately becomes $2k_0\,\text{Re}(n_{\text{eff}})L+\arg(r)+\arg(\rho+\tau)=2M\pi$ at $\omega=\text{Re}(\omega_{c,M})$. The latter is the already derived phase-matching condition for predicting resonance [5] and is related to a resonant excitation (i.e., constructive interference) of SPPs at real frequencies. In this sense, the resonant excitation of QNMs and that of SPPs for explaining the enhanced radiation are logically unified. For design tasks, this phase-matching condition provides an analytical expression to determine the antenna arm length L if the real resonance frequency $\text{Re}(\omega_{c,M})$ is prescribed.

B. Radiation Enhancement for an Emitter Located Near the Antenna Termination

As has been shown in Section 3.A, the antibonding modes do not contribute to the radiation of the emitter located in the nanogap. This can be also understood with the reciprocity between the source and the QNM [20] in view that the electric field of antibonding QNMs in the nanogap is nearly zero. To excite both the bonding and the antibonding modes, we place an x-polarized point emitter near one termination of the antenna, as shown in Fig. 4(a), where the distance between the emitter and the antenna termination is 15 nm. The unknown complex amplitude coefficients of SPPs are denoted by e_1, e_2, f_1, and f_2. They satisfy a set of coupled-mode equations,

$$f_1=e_1ur, \quad (15a)$$

$$f_2=\alpha+e_2ur, \quad (15b)$$

$$e_1=f_1u\rho+f_2u\tau, \quad (15c)$$

$$e_2=f_2u\rho+f_1u\tau, \quad (15d)$$

where α denotes the excitation coefficient of the SPP by the emitter [43] [see Fig. 4(b)] and can be calculated as the

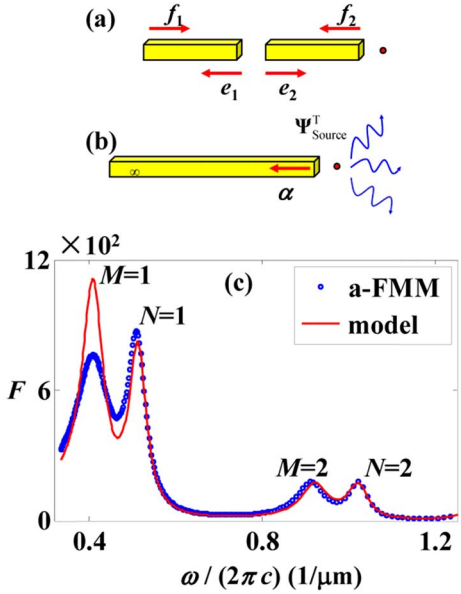

Fig. 4. (a) Definitions of the amplitude coefficients (e_1, e_2, f_1, and f_2) of SPPs excited by an x-polarized electric point source located near the antenna termination (with a distance of 15 nm). (b) Definitions of the SPP excitation coefficient α and scattered field Ψ^{T}_{Source} used in the model. (c) Enhancement factor F of radiation plotted as a function of illumination frequency $\omega/(2\pi c)$. Results are obtained with the full-wave a-FMM (blue circles) and the SPP model (red-solid curve), with antenna length $L=0.6$ μm.

scattering-matrix element [5,55] or with the Lorentzian reciprocity theorem [see Eqs. (C9) in Appendix C]. To solve Eqs. (15), we reformulate the unknown coefficients as $e_1+e_2=2e_+$, $e_1-e_2=2e_-$, $f_1+f_2=2f_+$, and $f_1-f_2=2f_-$, and the analytical solution can be obtained,

$$e_+=\frac{\alpha u(\rho+\tau)/2}{1-u^2r(\rho+\tau)}, \tag{16a}$$

$$e_-=-\frac{\alpha u(\rho-\tau)/2}{1-u^2r(\rho-\tau)}, \tag{16b}$$

$$f_+=\frac{\alpha/2}{1-u^2r(\rho+\tau)}, \tag{16c}$$

$$f_-=-\frac{\alpha/2}{1-u^2r(\rho-\tau)}. \tag{16d}$$

Then the excited field of the antenna can be expressed as

$$\mathbf{\Psi}=\mathbf{\Psi}^{\mathrm{T}}_{\mathrm{Source}}+e_1u\mathbf{\Psi}^{\mathrm{L,s}}_{\mathrm{SPP},-}+e_2u\mathbf{\Psi}^{\mathrm{R,s}}_{\mathrm{SPP},+}+f_1u\mathbf{\Psi}^{\mathrm{G,s}}_{\mathrm{SPP},+}+f_2u\mathbf{\Psi}^{\mathrm{G,s}}_{\mathrm{SPP},-}. \tag{17}$$

Equation (17) is written in a way similar to Eq. (1), except for the first term representing the source excitation [as sketched in Fig. 4(b)]. Inserting Eqs. (16) into Eq. (17), we obtain

$$\begin{aligned}\mathbf{\Psi}=\mathbf{\Psi}^{\mathrm{T}}_{\mathrm{Source}}&+\frac{\alpha/(2r)}{1-u^2r(\rho+\tau)}[u^2r(\rho+\tau)\mathbf{\Psi}^{\mathrm{L,s}}_{\mathrm{SPP},-}\\&+u^2r(\rho+\tau)\mathbf{\Psi}^{\mathrm{R,s}}_{\mathrm{SPP},+}+ur\mathbf{\Psi}^{\mathrm{G,s}}_{\mathrm{SPP},+}+ur\mathbf{\Psi}^{\mathrm{G,s}}_{\mathrm{SPP},-}]\\&+\frac{-\alpha/(2r)}{1-u^2r(\rho-\tau)}[u^2r(\rho-\tau)\mathbf{\Psi}^{\mathrm{L,s}}_{\mathrm{SPP},-}\\&-u^2r(\rho-\tau)\mathbf{\Psi}^{\mathrm{R,s}}_{\mathrm{SPP},+}+ur\mathbf{\Psi}^{\mathrm{G,s}}_{\mathrm{SPP},+}-ur\mathbf{\Psi}^{\mathrm{G,s}}_{\mathrm{SPP},-}].\end{aligned} \tag{18}$$

Then applying the complex pole expansion of meromorphic functions to Eq. (18) [with the use of Eqs. (3) and (4) for QNMs, as has been done for deriving Eqs. (13) and (14)], we finally obtain

$$\mathbf{\Psi}(\omega)=\sum_M\xi_M(\omega)\mathbf{\Psi}^{\mathrm{b}}_{\mathrm{QNM},M}+\sum_N\zeta_N(\omega)\mathbf{\Psi}^{\mathrm{a}}_{\mathrm{QNM},N}, \tag{19}$$

where ξ_M and ζ_N are complex expansion coefficients for the bonding ($\mathbf{\Psi}^{\mathrm{b}}_{\mathrm{QNM},M}$) and antibonding QNMs ($\mathbf{\Psi}^{\mathrm{a}}_{\mathrm{QNM},N}$), respectively, and are expressed as

$$\xi_M(\omega)=\frac{\omega/\omega_{c,M}}{\omega-\omega_{c,M}}\times\frac{(\alpha/2r)_{\omega=\omega_{c,M}}}{\left[-\frac{4\pi i\omega n_{\mathrm{eff}}L}{c}\left(\frac{1}{\omega}+\frac{1}{n_{\mathrm{eff}}}\frac{\partial n_{\mathrm{eff}}}{\partial\omega}\right)-\frac{1}{r}\frac{\partial r}{\partial\omega}-\frac{1}{\rho+\tau}\frac{\partial(\rho+\tau)}{\partial\omega}\right]_{\omega=\omega_{c,M}}}, \tag{20a}$$

$$\zeta_N(\omega)=\frac{\omega/\omega_{c,N}}{\omega-\omega_{c,N}}\times\frac{(\alpha/2r)_{\omega=\omega_{c,N}}}{\left[\frac{4\pi i\omega n_{\mathrm{eff}}L}{c}\left(\frac{1}{\omega}+\frac{1}{n_{\mathrm{eff}}}\frac{\partial n_{\mathrm{eff}}}{\partial\omega}\right)+\frac{1}{r}\frac{\partial r}{\partial\omega}+\frac{1}{\rho-\tau}\frac{\partial(\rho-\tau)}{\partial\omega}\right]_{\omega=\omega_{c,N}}}. \tag{20b}$$

Equation (19) shows that for an emitter located near the termination of the antenna, both the bonding and the antibonding QNMs contribute to the radiation [18,19]. Similar to the calculation of β in Eq. (14), with the use of reciprocity, α in Eqs. (20) for different emitter positions and polarizations can be obtained with only one full-wave calculation [see Eq. (C9) in Appendix C].

To check the validity of the SPP model, we plot the enhancement factor F as a function of frequency in Fig. 4(c). The results are obtained with the full-wave a-FMM (blue circles) and with Eqs. (19) and (20) of the model (red solid curves) for antenna length $L=0.6$ μm. Good agreement can be seen in the figure, except for a deviation at the resonance corresponding to the $M=1$ order QNM, which is due to the impact of surface waves other than SPPs (see Appendix A). Similar to the analysis in Section 3.A, Eqs. (19) and (20) show that the enhancement factor F peaks at $\omega=\mathrm{Re}(\omega_{c,M})$ and $\omega=\mathrm{Re}(\omega_{c,N})$, corresponding to the excitation of bonding and antibonding QNMs, respectively.

4. CONCLUSION

We build up an analytical model for the LSPR (i.e., QNM) of nanogap antennas by considering the multiple-scattering processes of SPPs that propagate back and forth on the antenna arms. The model integrates the advantages of the QNM approach and the Fabry–Perot model of SPPs and logically unifies the interpretations of the resonance behaviors of nanogap antennas with the two approaches. The existence of slightly damped QNMs for nanogap antennas is demonstrated with the model by seeking the solutions of two transcendental equations with the complex frequency as the unknown. The latter can be sometimes more computationally efficient than full-wave solvers of QNMs due to their uniqueness of solutions and analyticity with respect to the antenna arm length. The model demonstrates the fact that the QNM originates from a Fabry–Perot resonance of SPPs at the complex eigenfrequency. The bonding and the antibonding QNMs that possess different symmetries of field are explicitly discriminated with different analytical expressions. The predicted eigenfrequency slightly deviates from the full-wave a-FMM results for the lowest-order bonding QNM, unveiling the impact of surface waves other than SPPs to the antenna resonance.

With the assumption that the field of the antenna is a meromorphic function of frequency and by using the complex pole expansion theorem (Mittag–Leffler theorem), the field of the antenna under excitation by a nearby point emitter can be expanded with QNMs. With the model, the expansion coefficients and the mode volume of QNMs for calculating the Purcell factor are analytically expressed with the scattering coefficients of the SPP mode at the complex eigenfrequency of QNMs. The enhancement factor of radiation is shown to peak when the illumination frequency matches the real part of the complex eigenfrequency of QNMs, which is shown to be equivalent to a phase-matching condition that represents the Fabry–Perot resonance of SPPs. The present analysis of the LSPR with the SPP model establishes explicit relations between the concepts of LSPR and propagative SPP. The method can be extended to the analysis of other antenna structures, such as antennas with circular cross section [37,39], *L*-shaped antennas [48], cross antennas [45], split ring antennas [46,47], or antenna arrays [1]. For antennas with

arms of varying cross section such as bowtie antennas [49] or diabolo antennas [50], it could be possible to extend the present model by defining a SPP mode that propagates along the antenna arms adiabatically if the variation of the cross section is slow enough.

APPENDIX A: CALCULATION OF THE RESIDUAL FIELD AND ITS IMPACT ON THE ANTENNA RESONANCE

In the SPP model of LSPR, only the fundamental SPP mode is considered, and all other waves (composed of evanescent or unbounded waveguide modes) on the antenna arms are neglected. This is the reason why the model predictions of the eigenfrequencies of the $M = 1$ order QNM (Table 1) and of the enhancement factor of radiation in Figs. 3(c) and 4(c) at resonance corresponding to the $M = 1$ order QNM deviate from the full-wave a-FMM results. Here we provide the numerical data of the residual field on the antenna arms for different orders of QNMs and for the case that the antenna is illuminated by a point emitter. The residual field can be obtained by removing the SPP field from the total field.

For the QNM, the SPP field on the left arm of the antenna can be expressed as

$$\mathbf{\Psi}_{\mathrm{SPP}} = a\mathbf{\Psi}_{\mathrm{SPP},-} + b\mathbf{\Psi}_{\mathrm{SPP},+}, \tag{A1}$$

where $\mathbf{\Psi}_{\mathrm{SPP},\pm}$ denotes the fields of SPPs propagating along the positive and negative x directions and can be calculated with the a-FMM [5,52,53]. a and b can be extracted from the total field with the mode orthogonality theorem [36] or can be calculated with the a-FMM as the scattering matrix elements [55]. The residual field on the right arm of the antenna can be obtained in a similar way. The results for antenna length $L =$ 0.6 μm are shown in Fig. 5. It is seen that for the $M = 1$ order QNM, the residual field is comparable with the SPP field, so that the eigenfrequency predicted with the model deviates from the full-wave a-FMM results (see Table 1). For other orders of QNMs, the residual field is weak compared with the SPP field, so that the eigenfrequency predicted with the model is accurate. However, the field distribution of QNMs reproduced with the model agrees well with the a-FMM results even for the $M = 1$ order QNM. The reason is that we adopt the

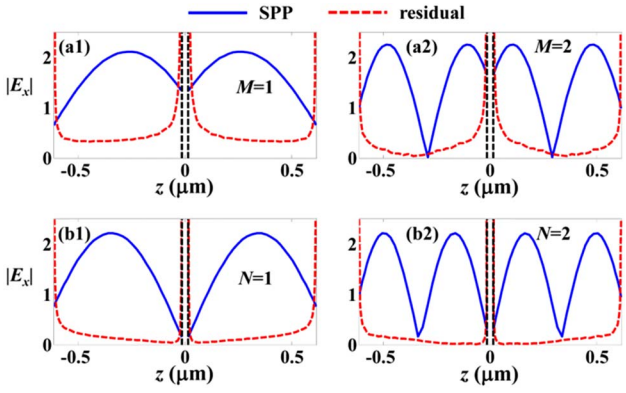

Fig. 5. SPP field and the residual field on the surface of the antenna arms for different orders of QNMs. (a1) and (a2) correspond to $M = 1$ and $M = 2$ orders of bonding QNMs, respectively. (b1) and (b2) correspond to $N = 1$ and $N = 2$ orders of antibonding QNMs, respectively. The results are obtained for antenna length $L = 0.6$ μm.

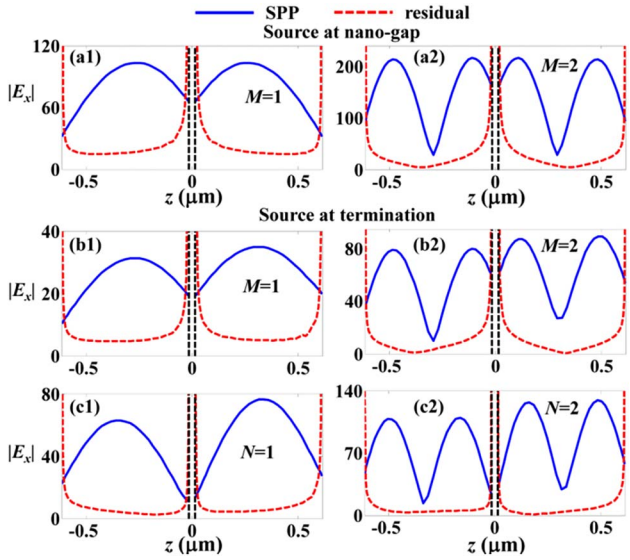

Fig. 6. SPP field and the residual field on the surface of the antenna arms at different resonance peaks of the enhancement factor F of radiation plotted in Figs. 3(c) and 4(c). (a1) and (a2) show the results at resonances corresponding to the $M = 1$ and $M = 2$ orders of QNMs for the case that the source is located at the center of the nanogap [see Fig. 3(c)]. (b1), (b2), (c1), and (c2) show the results at the resonances corresponding to $M = 1$, 2 and $N = 1$, 2 orders of QNMs for the case that the source is located near the antenna termination [see Fig. 4(c)]. The results are obtained for antenna length $L = 0.6$ μm.

normalization of $a = 1/u$ for the QNM field obtained with the a-FMM, which is consistent with the normalization of the QNM field obtained with the model [see Eqs. (4) in Section 2]. The residual field of the antenna is an analogue of the quasi-cylindrical wave on the flat metallic interface [65]. The latter has been shown to decay much faster than the SPP wave with the increase of the propagation distance, thus imposing a weaker impact on the electromagnetic interaction between scatterers with larger separation distance. Similarly, the relative ratio $L/\mathrm{Re}(\lambda_c)$ is larger for QNMs of higher orders (see the values of λ_c in Table 1), implying a weaker impact of the residual field on the antenna resonance (and resultingly, a higher accuracy of the SPP model).

For the case that the antenna is illuminated by a dipole source, the residual field on the antenna arms can be calculated similarly to Eq. (A1). The numerical results are shown in Fig. 6, where Fig. 6(a) is for the case that the source is located at the gap center (corresponding to Fig. 3), and Figs. 6(b) and 6(c) are for the case that the source is located near the antenna termination (corresponding to Fig. 4). It is seen that at the resonance corresponding to the $M = 1$ order QNM, the residual field is comparable with the SPP field, so that the enhancement factor F of radiation predicted with the model deviates from the full-wave a-FMM data, while at the resonances corresponding to other orders of QNMs, the residual field is weak and the results predicted with the model are accurate.

APPENDIX B: QNM FIELD AND RADIATION ENHANCEMENT OF NANOGAP ANTENNA WITH LENGTH $L = 0.2$ μm

For the nanogap antenna with arm length $L = 0.2$ μm, only $M = 1$ and $N = 1$ orders of QNMs need to be considered within the frequency range of interest. Their complex

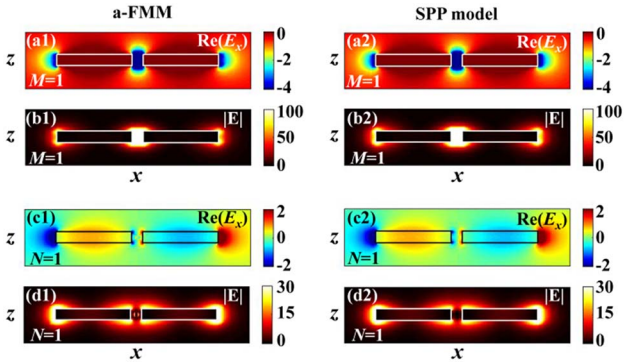

Fig. 7. Field distributions of QNMs for antenna length $L = 0.2$ μm. The left and right columns show the results obtained with the full-wave a-FMM and with the SPP model, respectively. (a) and (b) show the real part of E_x component and the amplitude of the electric field ($|\mathbf{E}| = \sqrt{|E_x|^2 + |E_y|^2 + |E_z|^2}$) for the $M = 1$ order QNM. (c) and (d) show the results for the $N = 1$ order QNM.

eigenfrequencies have been provided in Table 1. Here we provide the field of the $M = 1$ and $N = 1$ orders of QNMs for antenna length $L = 0.2$ μm. As shown in Fig. 7, the model predictions (right column) agree well with the full-wave a-FMM data (left column). For the bonding mode ($M = 1$), the field is concentrated in the nanogap and at terminations [Figs. 7(b1) and 7(b2)]. For the antibonding mode ($N = 1$), the field is concentrated at terminations but is nearly null in the nanogap [Figs. 7(d1) and 7(d2)]. The fields of the bonding mode and antibonding mode possess different symmetries [Figs. 7(a) and 7(c)]. These results are consistent with those of QNMs for antenna length $L = 0.6$ μm (Fig. 2).

The frequency response of the enhancement factor F for antenna length $L = 0.2$ μm is provided in Fig. 8. Figure 8(a) corresponds to the case that the point emitter is located at the center of the nanogap [as sketched in Fig. 3(a)], and Fig. 8(b) corresponds to the case that the point emitter is located near the antenna termination [as sketched in Fig. 4(a)]. It is seen that at the resonance peak corresponding to the $M = 1$ order QNM, the result obtained with the model (red curves) deviates from the a-FMM result (blue circles), which is due to the impact of the residual field other than SPPs. At the other resonance peak corresponding to the $N = 1$ order QNM, the enhancement factor predicted with the model is accurate.

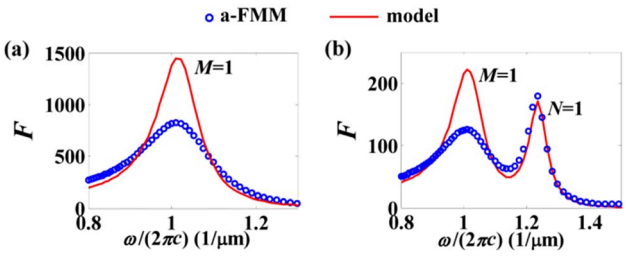

Fig. 8. Enhancement factor F of radiation plotted as a function of illumination frequency $\omega/(2\pi c)$ for antenna length $L = 0.2$ μm. The results are obtained with the full-wave a-FMM (blue circles) and the SPP model (red solid curves). (a) is for the case that the point emitter is located at the gap center [as sketched in Fig. 3(a)]. (b) is for the case that the point emitter is located near the antenna termination [as sketched in Fig. 4(a)].

APPENDIX C: ANALYTICAL EXPRESSION OF MODE VOLUME OF QNMS

The mode volume is an important quantity used in the calculation of the Purcell factor of a resonator [57]. However, calculation of the integral of the mode volume is a difficult task since the field of QNM diverges at infinity. It was recently shown that with the use of perfectly matched layers, the integral of the mode volume can be calculated in a rigorous manner [20]. Here we will show that with the SPP model, the mode volume can be expressed with the scattering coefficients and the complex effective index of the SPP.

We first consider the case that the point emitter is located at the gap center of the nanogap antenna, for which only the bonding QNM is excited. With the formalism developed in [20] based on the Lorentzian reciprocity theorem between a point emitter and the QNM, the expansion coefficient η_M of the excited field upon the basis of QNMs can be expressed as

$$\eta_M = \frac{\omega/\omega_{c,M}}{\omega - \omega_{c,M}} \frac{-i\mathbf{u}\cdot\tilde{\mathbf{E}}_b(\mathbf{r}_0)}{\int \left[\tilde{\mathbf{E}}_b \cdot \frac{\partial(\omega\varepsilon)}{\partial\omega}\tilde{\mathbf{E}}_b - \tilde{\mathbf{H}}_b \cdot \frac{\partial(\omega\mu)}{\partial\omega}\tilde{\mathbf{H}}_b\right]_{\omega=\omega_{c,M}} \mathrm{d}^3\mathbf{r}}, \quad \text{(C1)}$$

where $\tilde{\mathbf{E}}_b$ and $\tilde{\mathbf{H}}_b$ denote the electric- and magnetic-field vectors of the bonding QNM, $\mathbf{r}_0$ is the position coordinate of the electric point emitter, $\mathbf{u}$ is the unit vector along the polarization direction of the emitter ($\mathbf{u} = \mathbf{x}$ in our calculation), $\omega_{c,M}$ denotes the eigenfrequency of the Mth order bonding QNM, ω is the illumination frequency, and ε and μ are the dielectric constant and magnetic permeability, respectively. For deriving Eq. (C1), the complex pole expansion theorem of meromorphic functions is also applied (see Eq. (13) in [62] for more details). On the other hand, another analytical expression of η_M has been given by Eq. (14) of the model. Comparing the two equations, we obtain

$$\begin{aligned}\int \left[\tilde{\mathbf{E}}_b \cdot \frac{\partial(\omega\varepsilon)}{\partial\omega}\tilde{\mathbf{E}}_b - \tilde{\mathbf{H}}_b \cdot \frac{\partial(\omega\mu)}{\partial\omega}\tilde{\mathbf{H}}_b\right]_{\omega=\omega_{c,M}} \mathrm{d}^3\mathbf{r} \\ = \frac{-i\mathbf{u}\cdot\tilde{\mathbf{E}}_b(\mathbf{r}_0)}{(\beta u)_{\omega=\omega_{c,M}}} \left[-\frac{4\pi i\omega n_{\mathrm{eff}} L}{c}\left(\frac{1}{\omega} + \frac{1}{n_{\mathrm{eff}}}\frac{\partial n_{\mathrm{eff}}}{\partial\omega}\right)\right. \\ \left. - \frac{1}{r}\frac{\partial r}{\partial\omega} - \frac{1}{\rho+\tau}\frac{\partial(\rho+\tau)}{\partial\omega}\right]_{\omega=\omega_{c,M}}, \end{aligned} \quad \text{(C2)}$$

where n_{eff} is the complex effective index of the SPP. In [20], a generalized complex-valued mode volume of QNM is defined as

$$V_b = \frac{\int \left[\tilde{\mathbf{E}}_b \cdot \frac{\partial(\omega\varepsilon)}{\partial\omega}\tilde{\mathbf{E}}_b - \tilde{\mathbf{H}}_b \cdot \frac{\partial(\omega\mu)}{\partial\omega}\tilde{\mathbf{H}}_b\right]_{\omega=\omega_{c,M}} \mathrm{d}^3\mathbf{r}}{2\varepsilon_0[\mathbf{u}\cdot\tilde{\mathbf{E}}_b(\mathbf{r}_0)]^2}. \quad \text{(C3)}$$

Inserting Eq. (C2) into Eq. (C3), we finally obtain the expression of the mode volume for the bonding QNM,

$$V_b = \frac{\left[-\frac{4\pi i\omega n_{\mathrm{eff}} L}{c}\left(\frac{1}{\omega} + \frac{1}{n_{\mathrm{eff}}}\frac{\partial n_{\mathrm{eff}}}{\partial\omega}\right) - \frac{1}{r}\frac{\partial r}{\partial\omega} - \frac{1}{\rho+\tau}\frac{\partial(\rho+\tau)}{\partial\omega}\right]_{\omega=\omega_{c,M}}}{2i\varepsilon_0(\beta u)_{\omega=\omega_{c,M}}[\mathbf{u}\cdot\tilde{\mathbf{E}}_b(\mathbf{r}_0)]}. \quad \text{(C4)}$$

In Eq. (C4), the SPP excitation coefficient β [as sketched in Fig. 9(a)] can be calculated with the Lorentzian reciprocity theorem [36] between the emitter and the SPP mode. By considering a reciprocal scattering process of sending an incident

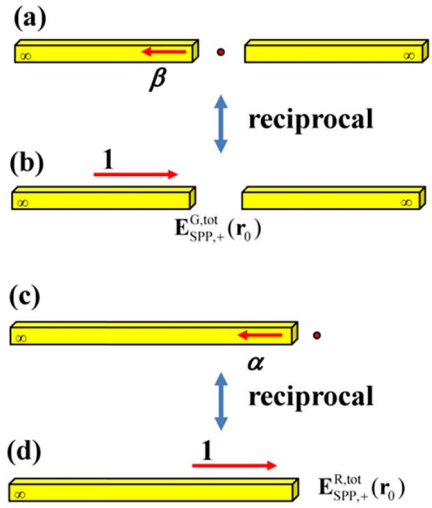

Fig. 9. Calculation of the SPP excitation coefficients β and α with the Lorentzian reciprocity theorem. (a) and (c) Definitions of the SPP excitation coefficients for the point emitter located in the nanogap and near the antenna termination, respectively. (b) and (d) Reciprocal scattering processes of (a) and (c) by sending an incident SPP toward the nanogap and toward the antenna termination, respectively. $\mathbf{E}^{\mathrm{G,tot}}_{\mathrm{SPP},+}(\mathbf{r}_0)$ and $\mathbf{E}^{\mathrm{R,tot}}_{\mathrm{SPP},+}(\mathbf{r}_0)$ in (b) and (d) denote the electric field at the source position $\mathbf{r}_0$ excited by the incident SPP.

SPP toward the nanogap [as sketched in Fig. 9(b)], β can be expressed as

$$\beta = \frac{\mathbf{u}\cdot\mathbf{E}^{\mathrm{G,tot}}_{\mathrm{SPP},+}(\mathbf{r}_0)}{\langle\boldsymbol{\Psi}_{\mathrm{SPP},+}|\boldsymbol{\Psi}_{\mathrm{SPP},-}\rangle}. \tag{C5}$$

In Eq. (C5), $\mathbf{E}^{\mathrm{G,tot}}_{\mathrm{SPP},+}(\mathbf{r}_0)$ denotes the electric field at the source position $\mathbf{r}_0$ excited by the incident SPP [as sketched in Fig. 9(b)], and the inner product in the denominator is defined as [36]

$$\langle\boldsymbol{\Psi}_{\mathrm{SPP},+}|\boldsymbol{\Psi}_{\mathrm{SPP},-}\rangle = \int_{-\infty}^{+\infty}\int_{-\infty}^{+\infty}[\mathbf{E}_{\mathrm{SPP},-}(x_0,y,z)\times\mathbf{H}_{\mathrm{SPP},+}(x_0,y,z) - \mathbf{E}_{\mathrm{SPP},+}(x_0,y,z)\times\mathbf{H}_{\mathrm{SPP},-}(x_0,y,z)]\cdot\mathbf{x}\mathrm{d}y\mathrm{d}z, \tag{C6}$$

where $\mathbf{E}_{\mathrm{SPP},\pm}$ and $\mathbf{H}_{\mathrm{SPP},\pm}$ are the electric and magnetic field vectors of two counterpropagating SPPs, and the value of the inner product is independent of the coordinate x_0 of the integral plane. As mentioned in Section 3, with the use of the reciprocity relation of Eq. (C5), the excitation coefficient β for different emitter positions $\mathbf{r}_0$ and polarizations $\boldsymbol{u}$ can be obtained with only one full-wave calculation of the field $\mathbf{E}^{\mathrm{G,tot}}_{\mathrm{SPP},+}(\mathbf{r}_0)$. This virtue with the use of reciprocity is analogous to that with the use of reciprocity between a point emitter and QNMs [20]. With Eq. (D5) (in Appendix D), $\tilde{\mathbf{E}}_{\mathrm{b}}(\mathbf{r}_0)$ in Eq. (C4) can be further simplified as

$$\tilde{\mathbf{E}}_{\mathrm{b}}(\mathbf{r}_0) = 2ur\mathbf{E}^{\mathrm{G,tot}}_{\mathrm{SPP},+}(\mathbf{r}_0), \tag{C7}$$

for which the symmetry of field at the central x-plane of the nanogap is used.

Next we consider the case that the source is located near the antenna termination. Now both the bonding and the antibonding QNMs will be excited. For the bonding QNM, similar to the derivation of Eq. (C4) and with the use of Eq. (20a) of the model, the mode volume can be expressed as

$$V_{\mathrm{b}} = \frac{\left[-\frac{4\pi i\omega n_{\mathrm{eff}}L}{c}\left(\frac{1}{\omega}+\frac{1}{n_{\mathrm{eff}}}\frac{\partial n_{\mathrm{eff}}}{\partial\omega}\right)-\frac{1}{r}\frac{\partial r}{\partial\omega}-\frac{1}{\rho+\tau}\frac{\partial(\rho+\tau)}{\partial\omega}\right]_{\omega=\omega_{c,M}}}{2i\varepsilon_0(\alpha/2r)_{\omega=\omega_{c,M}}[\mathbf{u}\cdot\tilde{\mathbf{E}}_{\mathrm{b}}(\mathbf{r}_0)]}. \tag{C8}$$

Similar to Eq. (C5) for β, by considering the reciprocal process of sending an incident SPP toward the antenna termination [as sketched in Fig. 9(d)], the SPP excitation coefficient α can be expressed as

$$\alpha = \frac{\mathbf{u}\cdot\mathbf{E}^{\mathrm{R,tot}}_{\mathrm{SPP},+}(\mathbf{r}_0)}{\langle\boldsymbol{\Psi}^{+}_{\mathrm{SPP}}|\boldsymbol{\Psi}^{-}_{\mathrm{SPP}}\rangle}, \tag{C9}$$

where $\mathbf{E}^{\mathrm{R,tot}}_{\mathrm{SPP},+}(\mathbf{r}_0)$ is the electric field at the source position $\mathbf{r}_0$ excited by sending a right-going SPP for a semi-infinitely long antenna [see Fig. 9(d)]. With the use of Eq. (D11) in the next section, the QNM field $\tilde{\mathbf{E}}_{\mathrm{b}}(\mathbf{r}_0)$ at the source position (near the antenna termination) in Eq. (C9) can be simplified as

$$\tilde{\mathbf{E}}_{\mathrm{b}}(\mathbf{r}_0) = \mathbf{E}^{\mathrm{R,tot}}_{\mathrm{SPP},+}(\mathbf{r}_0). \tag{C10}$$

For the antibonding QNM, the mode volume can be expressed as

$$V_{\mathrm{a}} = \frac{\left[\frac{4\pi i\omega n_{\mathrm{eff}}L}{c}\left(\frac{1}{\omega}+\frac{1}{n_{\mathrm{eff}}}\frac{\partial n_{\mathrm{eff}}}{\partial\omega}\right)+\frac{1}{r}\frac{\partial r}{\partial\omega}+\frac{1}{\rho-\tau}\frac{\partial(\rho-\tau)}{\partial\omega}\right]_{\omega=\omega_{c,M}}}{2i\varepsilon_0(\alpha/2r)_{\omega=\omega_{c,M}}[\mathbf{u}\cdot\tilde{\mathbf{E}}_{\mathrm{a}}(\mathbf{r}_0)]}. \tag{C11}$$

In Eq. (C11), the QNM field $\tilde{\mathbf{E}}_{\mathrm{a}}(\mathbf{r}_0)$ at the source position $\mathbf{r}_0$ can be simplified as

$$\tilde{\mathbf{E}}_{\mathrm{a}}(\mathbf{r}_0) = -\mathbf{E}^{\mathrm{R,tot}}_{\mathrm{SPP},+}(\mathbf{r}_0), \tag{C12}$$

for which Eq. (D12) in the next section is used.

APPENDIX D: SIMPLIFIED EXPRESSION OF QNM FIELD IN THE NANOGAP AND NEAR THE ANTENNA TERMINATION

The field of QNM expressed with Eq. (4) in Section 2 can be simplified in the horizontal region of the nanogap or away from the antenna termination. We first consider the horizontal region of the nanogap. For the third term in Eq. (4a) that expresses the bonding QNM, the field scattered by the nanogap can be expressed as

$$ur\boldsymbol{\Psi}^{\mathrm{G,s}}_{\mathrm{SPP},+} = ur(\boldsymbol{\Psi}^{\mathrm{G,tot}}_{\mathrm{SPP},+} - \boldsymbol{\Psi}^{\mathrm{G,inc}}_{\mathrm{SPP},+}), \tag{D1}$$

where $\boldsymbol{\Psi}^{\mathrm{G,tot}}_{\mathrm{SPP},+}$ is the total field excited by sending a right-going SPP from the left arm of an infinitely long nanowire with a nanogap [as sketched in Fig. 10(a)], and $\boldsymbol{\Psi}^{\mathrm{G,inc}}_{\mathrm{SPP},+}$ is the incident SPP field in the absence of the nanogap [Fig. 10(b)]. For the first term in Eq. (4a) and within the horizontal region of the nanogap, the field scattered by the left termination for an incident left-going SPP can be expressed as

$$\boldsymbol{\Psi}^{\mathrm{L,s}}_{\mathrm{SPP},-} = \boldsymbol{\Psi}^{\mathrm{L,tot}}_{\mathrm{SPP},-} - \boldsymbol{\Psi}^{\mathrm{L,inc}}_{\mathrm{SPP},-} = ur\boldsymbol{\Psi}^{\mathrm{G,inc}}_{\mathrm{SPP},+}, \tag{D2}$$

where $\Psi^{\mathrm{L,tot}}_{\mathrm{SPP},-}$ is the total field excited by sending a left-going SPP at a left-terminated semi-infinitely long nanowire [as sketched in Fig. 10(g)], and $\Psi^{\mathrm{L,inc}}_{\mathrm{SPP},-}$ is the incident SPP field at an infinitely long nanowire [Fig. 10(h)]. Equation (D2) is obtained in view that within the horizontal region of the nanogap, the scattered field is simply the reflected right-going SPP [multiplied by a phase shift $u = \exp(ik_{0,c}n_{\mathrm{eff}}L)$ and the SPP reflection coefficient r], as illustrated in Figs. 10(g) and 10(h). With Eqs. (D1) and (D2), we obtain

$$\Psi^{\mathrm{L,s}}_{\mathrm{SPP},-} + ur\Psi^{\mathrm{G,s}}_{\mathrm{SPP},+} = ur\Psi^{\mathrm{G,tot}}_{\mathrm{SPP},+}. \tag{D3}$$

Similarly, for the summation of the second and the last terms in Eq. (4a), we have

$$\Psi^{\mathrm{R,s}}_{\mathrm{SPP},+} + ur\Psi^{\mathrm{G,s}}_{\mathrm{SPP},-} = ur\Psi^{\mathrm{G,tot}}_{\mathrm{SPP},-}. \tag{D4}$$

With Eqs. (D3) and (D4) inserted into Eq. (4a), we finally obtain

$$\Psi^{\mathrm{b}}_{\mathrm{QNM}} = ur(\Psi^{\mathrm{G,tot}}_{\mathrm{SPP},+} + \Psi^{\mathrm{G,tot}}_{\mathrm{SPP},-}), \tag{D5}$$

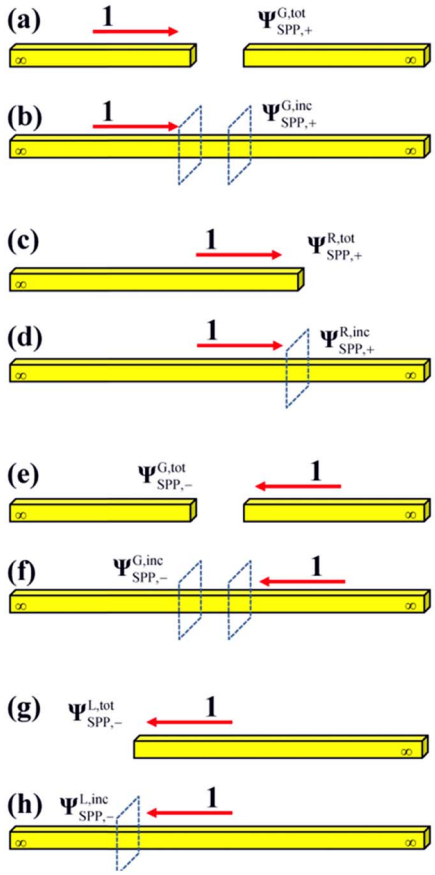

Fig. 10. (a) Total field $\Psi^{\mathrm{G,tot}}_{\mathrm{SPP},+}$ excited by a right-going SPP incident from the left arm of an infinitely long nanowire with a nanogap. (b) Incident right-going SPP field $\Psi^{\mathrm{G,inc}}_{\mathrm{SPP},+}$ in the absence of the scatterer of the nanogap. (c) Total field $\Psi^{\mathrm{R,tot}}_{\mathrm{SPP},+}$ excited by a right-going SPP at a right-terminated semi-infinitely long nanowire. (d) Incident right-going SPP field $\Psi^{\mathrm{R,inc}}_{\mathrm{SPP},+}$ at an infinitely long nanowire. (e)–(h) The same as (a)–(d) but for a left-going incident SPP.

which is valid within the horizontal region of the nanogap. In a parallel way, within the horizontal region of the nanogap, Eq. (4b), which expresses the antibonding QNM, can be simplified as

$$\Psi^{\mathrm{a}}_{\mathrm{QNM}} = ur(\Psi^{\mathrm{G,tot}}_{\mathrm{SPP},+} - \Psi^{\mathrm{G,tot}}_{\mathrm{SPP},-}). \tag{D6}$$

Next we consider the horizontal region on the right side of the right termination of the nanogap antenna. For the bonding QNM, the second term in Eq. (4a) is expressed as

$$\Psi^{\mathrm{R,s}}_{\mathrm{SPP},+} = \Psi^{\mathrm{R,tot}}_{\mathrm{SPP},+} - \Psi^{\mathrm{R,inc}}_{\mathrm{SPP},+}, \tag{D7}$$

where $\Psi^{\mathrm{R,tot}}_{\mathrm{SPP},+}$ is the total field excited by sending a right-going SPP at a right-terminated semi-infinitely long nanowire [as sketched in Fig. 10(c)], and $\Psi^{\mathrm{R,inc}}_{\mathrm{SPP},+}$ is the incident SPP field at an infinitely long nanowire [Fig. 10(d)]. The first term in Eq. (4a) can be simplified as

$$\Psi^{\mathrm{L,s}}_{\mathrm{SPP},-} = \Psi^{\mathrm{L,tot}}_{\mathrm{SPP},-} - \Psi^{\mathrm{L,inc}}_{\mathrm{SPP},-} = u^2vr\Psi^{\mathrm{R,inc}}_{\mathrm{SPP},+}, \tag{D8}$$

which is obtained in view that within the considered region, the scattered field is simply the reflected right-going SPP [multiplied by the SPP reflection coefficient r and a phase shift u^2v with $v = \exp(ik_{0,c}n_{\mathrm{eff}}w)$], as illustrated in Figs. 10(g) and 10(h). The third term in Eq. (4a) can be simplified as

$$ur\Psi^{\mathrm{G,s}}_{\mathrm{SPP},+} = ur(\Psi^{\mathrm{G,tot}}_{\mathrm{SPP},+} - \Psi^{\mathrm{G,inc}}_{\mathrm{SPP},+}) = ur(u\tau - uv)\Psi^{\mathrm{R,inc}}_{\mathrm{SPP},+}. \tag{D9}$$

The second equality of Eq. (D9) is obtained by using $\Psi^{\mathrm{G,tot}}_{\mathrm{SPP},+} = u\tau\Psi^{\mathrm{R,inc}}_{\mathrm{SPP},+}$ and $\Psi^{\mathrm{G,inc}}_{\mathrm{SPP},+} = uv\Psi^{\mathrm{R,inc}}_{\mathrm{SPP},+}$. Within the considered region, $\Psi^{\mathrm{G,tot}}_{\mathrm{SPP},+} = u\tau\Psi^{\mathrm{R,inc}}_{\mathrm{SPP},+}$ can be understood in view that the total field is simply the transmitted right-going SPP [multiplied by a phase shift u and the SPP transmission coefficient τ], as illustrated in Fig. 10(a). $\Psi^{\mathrm{G,inc}}_{\mathrm{SPP},+} = uv\Psi^{\mathrm{R,inc}}_{\mathrm{SPP},+}$ is obtained in view that $\Psi^{\mathrm{G,inc}}_{\mathrm{SPP},+}$ is simply the SPP field $\Psi^{\mathrm{R,inc}}_{\mathrm{SPP},+}$ at an infinitely long nanowire with a phase shift uv, as sketched in Figs. 10(b) and 10(d). The last term in Eq. (4a) can be simplified as

$$ur\Psi^{\mathrm{G,s}}_{\mathrm{SPP},-} = ur(\Psi^{\mathrm{G,tot}}_{\mathrm{SPP},-} - \Psi^{\mathrm{G,inc}}_{\mathrm{SPP},-}) = ur(u\rho\Psi^{\mathrm{R,inc}}_{\mathrm{SPP},+}), \tag{D10}$$

where $\Psi^{\mathrm{G,tot}}_{\mathrm{SPP},-}$ is the total field excited by sending a left-going SPP from the right arm of an infinitely long nanowire with a nanogap [as sketched in Fig. 10(e)], and $\Psi^{\mathrm{G,inc}}_{\mathrm{SPP},-}$ is the incident SPP field in the absence of the nanogap [Fig. 10(f)]. The second equality of Eq. (D10) can be understood in view of Figs. 10(e) and 10(f) (with ρ denoting the SPP reflection coefficient at the nanogap). With Eqs. (D7)–(D10) inserted into Eq. (4a) and with the use of Eq. (3a), we finally obtain,

$$\Psi^{\mathrm{b}}_{\mathrm{QNM}} = \Psi^{\mathrm{R,tot}}_{\mathrm{SPP},+}. \tag{D11}$$

Similarly, for the antibonding QNM, Eq. (4b) within the considered region can be simplified as

$$\Psi^{\mathrm{a}}_{\mathrm{QNM}} = -\Psi^{\mathrm{R,tot}}_{\mathrm{SPP},+}. \tag{D12}$$

Finally, we consider the horizontal region on the left side of the left termination of the nanogap antenna. Following the procedures for deriving Eqs. (D11) and (D12), we have

$$\Psi_{\mathrm{QNM}}^{\mathrm{b}} = \Psi_{\mathrm{SPP},-}^{\mathrm{L,tot}}, \tag{D13}$$

$$\Psi_{\mathrm{QNM}}^{\mathrm{a}} = \Psi_{\mathrm{SPP},-}^{\mathrm{L,tot}}. \tag{D14}$$

Funding. National Key Basic Research Program of China (2013CB328701); National Natural Science Foundation of China (NSFC) (61322508, 11504270).

Acknowledgment. Dr. Philippe Lalanne is acknowledged for providing helpful comments.

REFERENCES

1. R. M. Bakker, V. P. Drachev, Z. Liu, H. K. Yuan, R. H. Pedersen, A. Boltasseva, J. J. Chen, J. Irudayaraj, A. V. Kildishev, and V. M. Shalaev, "Nanoantenna array-induced fluorescence enhancement and reduced lifetimes," New J. Phys. **10**, 125022 (2008).
2. O. L. Muskens, V. Giannini, J. A. Sanchez-Gil, and J. Gómez Rivas, "Strong enhancement of the radiative decay rate of emitters by single plasmonic nanoantennas," Nano Lett. **7**, 2871–2875 (2007).
3. A. Kinkhabwala, Z. Yu, S. Fan, Y. Avlasevich, K. Müllen, and W. E. Moerner, "Large single-molecule fluorescence enhancements produced by a bowtie nanoantenna," Nat. Photonics **3**, 654–657 (2009).
4. A. V. Akimov, A. Mukherjee, C. L. Yu, D. E. Chang, A. S. Zibrov, P. R. Hemmer, H. Park, and M. D. Lukin, "Generation of single optical plasmons in metallic nanowires coupled to quantum dots," Nature **450**, 402–406 (2007).
5. H. Jia, H. Liu, and Y. Zhong, "Role of surface plasmon polaritons and other waves in the radiation of resonant optical dipole antennas," Sci. Rep. **5**, 8456 (2015).
6. X. W. Chen, V. Sandoghdar, and M. Agio, "Coherent interaction of light with a metallic structure coupled to a single quantum emitter: from superabsorption to cloaking," Phys. Rev. Lett. **110**, 153605 (2013).
7. P. Mühlschlegel, H. J. Eisler, O. J. F. Martin, B. Hech, and D. W. Pohl, "Resonant optical antennas," Science **308**, 1607–1609 (2005).
8. Z. Liu, E. Li, V. M. Shalaev, and A. V. Kildishev, "Near field enhancement in silver nanoantenna–superlens systems," Appl. Phys. Lett. **101**, 021109 (2012).
9. H. Fischer and O. J. Martin, "Polarization sensitivity of optical resonant dipole antennas," J. Eur. Opt. Soc. **3**, 08018 (2008).
10. L. Novotny and N. Van Hulst, "Antennas for light," Nat. Photonics **5**, 83–90 (2011).
11. H. Jia, P. Lalanne, and H. Liu, "Comprehensive surface-wave description for the nano-scale energy concentration with resonant dipole antennas," Plasmonics **11**, 1025–1033 (2016).
12. R. Esteban, G. Aguirregabiria, A. G. Borisov, Y. M. Wang, P. Nordlander, G. W. Bryant, and J. Aizpurua, "The morphology of narrow gaps modifies the plasmonic response," ACS Photon. **2**, 295–305 (2015).
13. T. Hanke, G. Krauss, D. Träutlein, B. Wild, R. Bratschitsch, and A. Leitenstorfer, "Efficient nonlinear light emission of single gold optical antennas driven by few-cycle near-infrared pulses," Phys. Rev. Lett. **103**, 257404 (2009).
14. H. Harutyunyan, G. Volpe, R. Quidant, and L. Novotny, "Enhancing the nonlinear optical response using multifrequency gold-nanowire antennas," Phys. Rev. Lett. **108**, 217403 (2012).
15. W. Zhang, H. Fischer, T. Schmid, R. Zenobi, and O. J. Martin, "Mode-selective surface-enhanced Raman spectroscopy using nanofabricated plasmonic dipole antennas," J. Phys. Chem. C **113**, 14672–14675 (2009).
16. F. Jäckel, A. A. Kinkhabwala, and W. E. Moerner, "Gold bowtie nanoantennas for surface-enhanced Raman scattering under controlled electrochemical potential," Chem. Phys. Lett. **446**, 339–343 (2007).
17. K. Höflich, M. Becker, G. Leuchs, and S. Christiansen, "Plasmonic dimer antennas for surface enhanced Raman scattering," Nanotechnology **23**, 185303 (2012).
18. M. Liu, T. W. Lee, S. K. Gray, P. Guyot-Sionnest, and M. Pelton, "Excitation of dark plasmons in metal nanoparticles by a localized emitter," Phys. Rev. Lett. **102**, 107401 (2009).
19. J. S. Huang, J. Kern, P. Geisler, P. Weinmann, M. Kamp, A. Forchel, P. Biagioni, and B. Hecht, "Mode imaging and selection in strongly coupled nanoantennas," Nano Lett. **10**, 2105–2110 (2010).
20. C. Sauvan, J. P. Hugonin, I. S. Maksymov, and P. Lalanne, "Theory of the spontaneous optical emission of nanosize photonic and plasmon resonators," Phys. Rev. Lett. **110**, 237401 (2013).
21. J. Yang, H. Giessen, and P. Lalanne, "Simple analytical expression for the peak-frequency shifts of plasmonic resonances for sensing," Nano Lett. **15**, 3439–3444 (2015).
22. E. S. C. Ching, P. T. Leung, A. M. van den Brink, W. M. Suen, S. S. Tong, and K. Young, "Quasinormal-mode expansion for waves in open systems," Rev. Mod. Phys. **70**, 1545–1554 (1998).
23. Q. Bai, M. Perrin, C. Sauvan, J. P. Hugonin, and P. Lalanne, "Efficient and intuitive method for the analysis of light scattering by a resonant nanostructure," Opt. Express **21**, 27371–27382 (2013).
24. R. C. Ge, P. T. Kristensen, J. F. Young, and S. Hughes, "Quasinormal mode approach to modelling light-emission and propagation in nanoplasmonics," New J. Phys. **16**, 113048 (2014).
25. C. Sauvan, J. P. Hugonin, R. Carminati, and P. Lalanne, "Modal representation of spatial coherence in dissipative and resonant photonic systems," Phys. Rev. A **89**, 043825 (2014).
26. R. C. Ge, J. F. Young, and S. Hughes, "Quasi-normal mode approach to the local-field problem in quantum optics," Optica **2**, 246–249 (2015).
27. P. T. Leung, Y. T. Liu, C. Y. Tam, and K. Young, "Numerical solution for quasinormal modes for potentials with exponential tails," Phys. Lett. A **247**, 253–260 (1998).
28. J. Wiersig, "Boundary element method for resonances in dielectric microcavities," J. Opt. A **5**, 53–60 (2003).
29. M. B. Doost, W. Langbein, and E. A. Muljarov, "Resonant-state expansion applied to three-dimensional open optical systems," Phys. Rev. A **90**, 013834 (2014).
30. P. T. Leung, S. Y. Liu, and K. Young, "Completeness and orthogonality of quasinormal modes in leaky optical cavities," Phys. Rev. A **49**, 3057–3067 (1994).
31. E. A. Muljarov, W. Langbein, and R. Zimmermann, "Brillouin–Wigner perturbation theory in open electromagnetic systems," Europhys. Lett. **92**, 50010 (2010).
32. M. S. Eggleston, K. Messer, L. Zhang, E. Yablonovitch, and M. C. Wu, "Optical antenna enhanced spontaneous emission," Proc. Natl. Acad. Sci. USA **112**, 1704–1709 (2015).
33. A. Alù and N. Engheta, "Input impedance, nanocircuit loading, and radiation tuning of optical nanoantennas," Phys. Rev. Lett. **101**, 043901 (2008).
34. A. Artar, A. A. Yanik, and H. Altug, "Directional double Fano resonances in plasmonic hetero-oligomers," Nano Lett. **11**, 3694–3700 (2011).
35. R. Adato and H. Altug, "In-situ ultra-sensitive infrared absorption spectroscopy of biomolecule interactions in real time with plasmonic nanoantennas," Nat. Commun. **4**, 2154 (2013).
36. C. Vassallo, *Optical Waveguide Concepts* (Elsevier, 1991).
37. D. E. Chang, A. S. Sørensen, P. R. Hemmer, and M. D. Lukin, "Strong coupling of single emitters to surface plasmons," Phys. Rev. B **76**, 035420 (2007).
38. H. Liu, "Coherent-form energy conservation relation for the elastic scattering of a guided mode in a symmetric scattering system," Opt. Express **21**, 24093–24098 (2013).
39. R. Gordon, "Reflection of cylindrical surface waves," Opt. Express **17**, 18621–18629 (2009).
40. A. Aubry, D. Y. Lei, S. A. Maier, and J. B. Pendry, "Interaction between plasmonic nanoparticles revisited with transformation optics," Phys. Rev. Lett. **105**, 233901 (2010).
41. T. H. Taminiau, F. D. Stefani, and N. F. van Hulst, "Optical nanorod antennas modeled as cavities for dipolar emitters: evolution of sub- and super-radiant modes," Nano Lett. **11**, 1020–1024 (2011).
42. L. Douillard, F. Charra, Z. Korczak, R. Bachelot, S. Kostcheev, G. Lerondel, P. M. Adam, and P. Royer, "Short range plasmon

resonators probed by photoemission electron microscopy," Nano Lett. **8**, 935–940 (2008).
43. C. Liu, H. Liu, and Y. Zhong, "Impact of surface plasmon polaritons and other waves on the radiation of a dipole emitter close to a metallic nanowire antenna," Opt. Express **22**, 25539–25549 (2014).
44. J. Dorfmuller, R. Vogelgesang, W. Khunsin, C. Rockstuhl, C. Etrichm, and K. Kern, "Plasmonic nanowire antennas: experiment, simulation, and theory," Nano Lett. **10**, 3596–3603 (2010).
45. P. Biagioni, J. S. Huang, L. Duò, M. Finazzi, and B. Hecht, "Cross resonant optical antenna," Phys. Rev. Lett. **102**, 256801 (2009).
46. J. Scheuer, "Ultra-high enhancement of the field concentration in split ring resonators by azimuthally polarized excitation," Opt. Express **19**, 25454–25464 (2011).
47. E. Cubukcu, S. Zhang, Y. S. Park, G. Bartal, and X. Zhang, "Split ring resonator sensors for infrared detection of single molecular monolayers," Appl. Phys. Lett. **95**, 043113 (2009).
48. S. C. Jiang, X. Xiong, Y. S. Hu, Y. H. Hu, G. B. Ma, R. W. Peng, C. Sun, and M. Wang, "Controlling the polarization state of light with a dispersion-free metastructure," Phys. Rev. X **4**, 021026 (2014).
49. X. Zhang, C. J. Chung, S. Wang, H. Subbaraman, Z. Pan, Q. Zhan, and R. T. Chen, "Integrated broadband bowtie antenna on transparent silica substrate," IEEE Antennas Wireless Propag. Lett. **15**, 1377–1381 (2016).
50. Z. Pan and J. Guo, "Enhanced optical absorption and electric field resonance in diabolo metal bar optical antennas," Opt. Express **21**, 32491–32500 (2013).
51. E. D. Palik, *Handbook of Optical Constants of Solids Part II* (Academic, 1985).
52. J. P. Hugonin and P. Lalanne, "Perfectly matched layers as nonlinear coordinate transforms: a generalized formalization," J. Opt. Soc. Am. A **22**, 1844–1849 (2005).
53. The calculation is performed with in-house software, H. Liu, *DIF CODE for Modeling Light Diffraction in Nanostructures* (Nankai University, 2010).
54. M. Besbes, J. P. Hugonin, P. Lalanne, S. van Haver, O. T. A. Janssen, A. M. Nugrowati, M. Xu, S. F. Pereira, H. P. Urbach, A. S. van de Nes, P. Bienstman, G. Granet, A. Moreau, S. Helfert, M. Sukharev, T. Seideman, F. I. Baida, B. Guizal, and D. Van Labeke, "Numerical analysis of a slit-groove diffraction problem," J. Eur. Opt. Soc. **2**, 07022 (2007).
55. L. Li, "Formulation and comparison of two recursive matrix algorithms for modeling layered diffraction gratings," J. Opt. Soc. Am. A **13**, 1024–1035 (1996).
56. Y. Li, H. Liu, H. Jia, F. Bo, G. Zhang, and J. Xu, "Fully-vectorial modeling of cylindrical microresonators with aperiodic Fourier modal method," J. Opt. Soc. Am. A **31**, 2459–2466 (2014).
57. E. M. Purcell, "Spontaneous emission probabilities at radio frequencies," Phys. Rev. **69**, 37–38 (1946).
58. E. Knill, R. Laflamme, and G. J. Milburn, "A scheme for efficient quantum computation with linear optics," Nature **409**, 46–52 (2001).
59. M. Agio, "Optical antennas as nanoscale resonators," Nanoscale **4**, 692–706 (2012).
60. P. T. Leung, S. S. Tong, and K. Young, "Two-component eigenfunction expansion for open systems described by the wave equation I: completeness of expansion," J. Phys. A **30**, 2139–2151 (1997).
61. P. T. Leung, S. S. Tong, and K. Young, "Two-component eigenfunction expansion for open systems described by the wave equation II: linear space structure," J. Phys. A **30**, 2153–2162 (1997).
62. F. Yang, H. Liu, H. Jia, and Y. Zhong, "Analytical description of quasi normal mode in resonant plasmonic nano-cavities," J. Opt. **18**, 035003 (2016).
63. G. B. Arfken, *Mathematical Methods for Physicists* (Elsevier, 2005).
64. M. B. Doost, W. Langbein, and E. A. Muljarov, "Resonant state expansion applied to two-dimensional open optical systems," Phys. Rev. A **87**, 043827 (2013).
65. F. van Beijnum, C. Rétif, C. B. Smiet, H. Liu, P. Lalanne, and M. P. van Exter, "Quasi-cylindrical wave contribution in experiments on extraordinary optical transmission," Nature **492**, 411–414 (2012).